HHS Public Access

Author manuscript

J Cell Biochem. Author manuscript; available in PMC 2023 March 01.

Published in final edited form as:

J Cell Biochem. 2022 March ; 123(3): 568–580. doi:10.1002/jcb.30204.

Glycosylation of FGFR4 in cholangiocarcinoma regulates receptor processing and cancer signaling

Andrew J. Phillips[1], **Marissa B. Lobl**[1], **Yamnah A. Hafeji**[2], **Hannah R. Safranek**[2], **Ashley M. Mohr**[2], **Justin L. Mott**[2]

[1]Cancer Research Doctoral Program, Fred & Pamela Buffet Cancer Center

[2]Department of Biochemistry and Molecular Biology, Fred & Pamela Buffett Cancer Center, University of Nebraska Medical Center

Abstract

Recent advances in targeted treatment for cholangiocarcinoma have focused on fibroblast growth factor (FGF) signaling. There are four receptor tyrosine kinases that respond to FGF's, and posttranslational processing has been demonstrated for each FGF receptor. Here, we investigated the role of N-linked glycosylation on processing and function of FGFR4. We altered glycosylation through enzymatic deglycosylation, small molecule inhibition of glycosyltransferases, or through site-directed mutagenesis of selected asparagine residues in FGFR4. Signaling was tested through caspase activation, migration, and subcellular localization of FGFR4. Our data demonstrate that FGFR4 has multiple glycoforms, with predominant bands relating to the full-length receptor that has a high mannose- or hybrid-type form and a complex-type glycan form. We further identified a set of faster migrating FGFR4 bands that correspond to the intracellular kinase domain, termed R4-ICD. These glycoforms and R4-ICD were detected in human cholangiocarcinoma tumor samples, where R4-ICD was predominant. Removal of glycans in intact cells by enzymatic deglycosylation resulted in increased processing to R4-ICD. Inhibition of glycosylation using NGI-1, an oligosaccharyltransferase inhibitor, reduced both high mannose- or hybrid- and complex-type glycan forms of FGFR4, increased processing, and sensitized to apoptosis. Mutation of Asn-112, Asn-258, Asn-290, or Asn-311 to glutamine modestly reduced apoptosis resistance, while mutation of Asn-322 or simultaneous mutation of the other four asparagine residues caused a loss of cytoprotection by FGFR4. None of the glycomutants altered migration of cancer cells. Finally, mutation of Asn-112 caused a partial localization of FGFR4 to the Golgi. Overall, preventing glycosylation at individual residues reduced the cell survival function of FGFR4 and receptor glycosylation may regulate access to an extracellular protease or proteolytic susceptibility of FGFR4.

Address for correspondence: Justin L. Mott, MD, PhD, 985870 Nebraska Medical Center, Omaha, NE, 68198-5870, 402-559-3177, justin.mott@unmc.edu.

Author Contributions:

AJP designed and performed experiments, analyzed the data, and prepared the manuscript. MBL, YAH, HRS performed experiments and analyzed data. AMM designed experiments, analyzed data, and edited the manuscript. JLM designed experiments, analyzed and interpreted data, and edited and revised the manuscript.

Conflict of Interests:

The authors declare that there are no conflicts of interests.

Keywords

Apoptotic; bile duct; biliary tract cancer; FGF19; glycoprotein

Introduction:

Cholangiocarcinoma is a primary liver cancer of the epithelial cells lining the biliary tract. Cholangiocarcinoma commonly presents late in disease and patients have a very poor prognosis; less than 10% 5-year survival (Razumilava, et al., 2014).

Treatment options include newly approved small molecule inhibitors targeting FGFRs, isocitrate dehydrogenase, and ROS proto-oncogene 1 (Massironi, et al., 2020; Rizvi, et al., 2018). However, many of these treatment options are only approved for a select group of patients. As such, gemcitabine plus cisplatin remains a common first-line therapy (Valle, et al., 2010). In the meantime, finding new therapeutic targets in cholangiocarcinoma remains a top priority.

One such group of therapeutic targets includes receptor tyrosine kinases, such as fibroblast growth factor receptors (FGFR). FGFR4 is involved in the regulation of bile acid synthesis. In cancer biology, FGFR4 has been shown to play a role in malignant signaling through its overexpression. This has been observed in various tumors including breast, lung, gastric cancers, rhabdomyosarcoma, nasopharyngeal carcinoma, and cholangiocarcinoma (Meijer, et al., 2008; Tiong, et al., 2016; Taylor, et al., 2009; Xu, et al., 2014).

There are five FGFRs (only four with functional kinase domains) and twenty-three FGF ligands (Ornitz, et al., 2015). FGF19 is expressed in biliary tissue and is amplified in 4–6% of cholangiocarcinomas (Lee, et al., 2004; Sia, et al., 2013; Vasilieva, et al., 2013; Nakamura, et al., 2015). FGF19's receptor, FGFR4, is also expressed in cholangiocarcinoma. Ligand binding occurs between the second and third immunoglobulin loop structures. In the presence of the coreceptor, beta klotho, receptor dimerization can occur and autophosphorylation of the FGFR kinase domain follows (Lin, et al., 2007; Wu, et al., 2007). N-linked glycosylation of FGFR4 plays a role in FGFR4 localization and signaling (Triantis, et al., 2010; Tuominen, et al., 2001).

Some similarities exist between Notch and FGFR family protein, FGFR3. Dysregulation of Notch signaling has been implicated in cancer. Notch3 overexpression was observed in approximately 40% of non-small cell lung cancers. Often, this was observed with reduced manic fringe expression. Manic fringe is one of the three human glycosyltransferases that modify Notch proteins (Taylor, et al., 2014; Takeuchi, et al., 2014). When manic fringe expression was restored, Notch3 was destabilized, and tumor growth was reduced (Yi, et al., 2013). FGFR3 has been shown to undergo regulated intramembrane proteolysis upon ligand binding. S1 cleavage occurs, releasing the extracellular domain. The membrane-anchored remaining portion of FGFR3 undergoes a second cleavage event, S2, which effectively releases the intracellular domain from the plasma membrane, allowing nuclear translocation. Like what is observed in Notch signaling, FGFR3 activation (receptor phosphorylation) is required for proteolysis to occur (Degnin, et al., 2011). FGFR4 has five extracellular

asparagine residues which match the Asn-X-Ser/Thr sequon (where X is not proline) required for N-linked glycosylation to occur. These asparagine residues are located at positions 112, 258, 290, 311, and 322. The current study investigated the functional role of FGFR4 glycosylation in cholangiocarcinoma and the effects of glycosylation on processing to R4-ICD.

Methods:

Cell culture:

Human malignant cholangiocarcinoma cells, KMCH, Mz-ChA-1, and HuCCT1, were kindly provided by Dr. Gregory Gores. Cells were cultured in high-glucose DMEM supplemented with 10% fetal bovine serum, G418 (50 μg/mL), and insulin (0.5 μg/mL). FGFR4 plasmids were generously provided by Dr. Javed Khan (National Cancer Institute) and have been described previously (Taylor, et al., 2009). HuCCT1 cells were transfected and selected with puromycin (2–10 μg/mL). Single-cell colonies were isolated.

Immunoblotting:

Cells were lysed by the addition of 50 mM Tris-HCl, 150 mM NaCl, 1 mM EDTA, 1 mM dithiothreitol, 1 mM α-phenylmethylsulfonyl fluoride, 1 mM Na_3VO_4, 100 mM NaF, and 1% Triton X-100, pH 7.4. Following SDS-PAGE and transfer to nitrocellulose membrane, FGFR4 signal was detected via immunoblotting: Cell Signaling Technology (FGFR4: #8562) or Sigma Aldrich (Actin: A2228). Antibody specificity was verified via the molecular weight of FGFR4, a decrease in signal upon use of an siRNA against FGFR4 (not shown), and restored signal with transfection of an FGFR4 expression plasmid.

Post-translational modifications:

Glycosylation was altered by enzyme-mediated deglycosylation, inhibition of glycosyltransferases, or site-directed mutagenesis. PNGase F and Endoglycosidase H were from New England Biolabs (PNGase F: P0704S, Endoglycosidase H: P0702S). NGI-1 (Selleckchem: S8750) and added to cells at 0–100 μM, overnight. Kifunensine (Cayman Chemical: 10009437) was used at 5 μM final concentration for the indicated times.

Enzyme-mediated deglycosylation, lysate: Cells were lysed in the manufacturer-supplied lysis buffer that contained 10% NP-40. Lysate was vortexed briefly three times, and placed on ice between each. Lysate was centrifuged (13,000*g*, 5 min) and supernatant saved. The supernatant (5 μL) was incubated under native or denaturing conditions, per the manufacturer and the reaction started by addition of 500 units of enzyme. The reaction was terminated with one volume of 2X Laemmli buffer and heated to 95°C for 5 min.

Enzyme-mediated deglycosylation, live cells: Cells were plated at 70–80% confluency in a 12-well plate. Media was replaced with Opti-MEM media (ThermoFisher Scientific: 22600050) containing 5,000 units of PNGase F per mL for 1–4 hours. Protein was isolated for immunoblotting, as above.

Phosphatase: The manufacturer's protocol was used (New England Biolabs, Lambda Protein Phosphatase: P0753S), with modification. Protein isolation and denaturation steps

were identical to those performed in the PNGase F denatured lysate protocol. Following deglycosylation, 2 μL of protein metallophosphatase (PMP) buffer, 2 μL of 10 mM $MnCl_2$ and 6 μL of water were added to the 10 μL sample to give a total reaction volume of 20 μL. PNGase F or Lambda phosphatase (1 μL each), were added and incubated at 30°C for 1 hour.

Site-directed mutagenesis:

Agilent QuikChange Lightning, 210519, or New England Biolabs Q5 Site-Directed Mutagenesis, E0554, were used to replace each of the five predicted glycosylation residues (Asn-112, −258, −290, −311, −322) to convert asparagine to glutamine. All mutations were confirmed through sequencing.

Active lysate isolation:

We measured receptor cleavage of FGFR4 full-length protein to R4-ICD, in the absence of protein synthesis and glycosylation, in crude lysate, inspired by reports using crude cell lysate to measure endogenous enzyme activity (Arauz, et al., 2016; Rodgers, et al., 2003). Cells were mechanically lysed in hypotonic non-denaturing lysis buffer (30 mM NaCl, 20 mM Tris, pH 7.4), either by Dounce homogenization (larger volumes) or needle shearing (small samples). Initial experiments on the same sample demonstrated no difference between these methods. Dounce homogenization (glass/ground glass) was done with 20 passes per sample and needle shearing with 20 passes through a 29-gauge needle. Lysates were either frozen immediately or incubated at 37°C. Processing was arrested by adding Laemmli buffer and heating to 95°C for 5-minutes.

Migration:

Cells were plated at 5,000 cells/well into transwell inserts in serum-free media (Sigma, CLS3422–48EA) with media containing 10% fetal bovine serum in the lower chamber. At 24 hours, non-migrated cells were removed and the insert processed (Justus, et al., 2014). Cells from five non-overlapping images (field of view was 1 mm x 1.4 mm) per insert were counted using CellProfiler (CellProfiler pipeline has been included in the supplementary information).

Caspase activity:

Caspase 3/7 activity was measured by quantifying the release of Rhodamine-110 from the peptide DEVD (Promega: G7792) according to the manufacturer's instructions, with quadruplicates of each group. Cells were treated as in figure legends. The following day, apoptosis was stimulated with 10 ng/mL TNF-related apoptosis-inducing ligand (R&D Systems, 375-TL-010) for 6 hours. Alternatively, apoptosis was stimulated with Cisplatin (Fresenius Kabi: 63323–103-51) and gemcitabine (Zydus Hospira Oncology: 0409–0185-01) at 50 and 5 μM respectively, or staurosporine (Fisher Scientific: BP2541–100) at 2 ng/mL for 24 hours.

FGFR4 localization:

Cells plated on collagen-coated coverslips were fixed in 3% paraformaldehyde in dPBS with 100 mM PIPES, 3 mM $MgSO_4$ & 1 mM EGTA then permeabilized in 0.1% Triton X-100 in dPBS. Primary antibodies (Protein-Tech anti-FGFR4, 1:50: 11098–1-AP, Cell Signaling anti-FGFR4, 1:100: #8562, or Abcam anti-giantin, 1:50: ab37266). Secondary antibody (Thermo Fisher, donkey anti-rabbit, 594 nm: A21207, donkey anti-rabbit, 488 nm, donkey anti-mouse, 488 nm: A21202) was added (1:2,000, FGFR4 or 1:200, Giantin) for 45 minutes at room temperature. Samples were mounted in ProLong Gold with DAPI. Zeiss LSM 800 with Airyscan was used for confocal imaging.

Results:

FGFR4 glycosylation in cholangiocarcinoma

N-linked glycosylation is predicted to occur at five residues in FGFR4 (Figure 1A). Cholangiocarcinoma cell lines, HuCCT1-FGFR4 and KMCH, demonstrated two predominant FGFR4 forms running at roughly 90 and 110 kDa on immunoblot, plus signal at 45–50 kDa, consistent with the predicted size of the intracellular domain (amino acids 391–802). The faster migrating forms (45–50 kDa) were collectively termed R4-intracellular domain (R4-ICD) based on size and immunoreactivity to the C-terminal anti-FGFR4 antibody. R4-ICD was absent in cells lacking full-length FGFR4 (HuCCT1 parental) and was restored upon transfection with FGFR4 (HuCCT1-FGFR4; Figure 1B). Because we observed R4-ICD in HuCCT1 cells transfected with cDNA for FGFR4, and cDNA is not a substrate for splicing, we reasoned that R4-ICD is not alternative splice variant. Similar 45–50 kDa forms of FGFR4 have been demonstrated, although their function has not been studied (Merilahti, et al., 2017; Huang, et al., 2009). In summary, FGFR4 protein showed multiple forms with the 90–100 kDa forms potentially representing glycosylated receptor and the faster migrating R4-ICD forms likely representing proteolytically processed FGFR4. The level of R4-ICD signal relative to full-length showed variability, suggestive of regulation.

FGFR4 in human liver tissue and cholangiocarcinoma

FGFR4 in human cholangiocarcinoma was investigated from archived, frozen tumor samples. Samples were from 3 normal livers adjacent to tumor, 3 non-tumor livers, and 14 tumors, including 6 male and 8 female patients. One cancer patient was 32 years old, the rest were in the range of 50–72 years, with an average age of 60 (Table 1). Occasional protein samples from frozen human tissue appear to have been poorly preserved, showing signs of protein aggregation and degradation on immunoblot (smearing of FGFR4 signal, weak actin, e.g., lane 4). Lane numbers indicated below Figure 1C correspond to tumor samples numbered in the “Lane” column of Table 1. R4-ICD signal was stronger than full-length FGFR4 in human samples, and R4-ICD was observed in all 14 of the tumor samples. The lighter exposure blot demonstrated substantially higher levels of R4-ICD in tumor samples compared to non-tumor. Robust signal from full-length FGFR4 was observed in 12 of 14 tumor samples, but only 3 out of 6 normal tissues. Note that one tumor-adjacent sample (lane 4) was likely poorly preserved and exhibited a strong signal without distinct banding for FGFR4. Overall, tumor samples showed high levels of FGFR4 and R4-ICD (Figure 1C).

FGFR4 glycosylation was examined by treatment with Endoglycosidase H to remove high mannose- and hybrid-type N-glycans. Endoglycosidase H caused a shift of the 90 kDa band to two faster migrating bands at approximately 80–85 kDa. The 90 kDa band was fully susceptible to Endoglycosidase H processing, indicating that this band represents the high mannose- and/or hybrid-type N-glycosylated forms while the 110 kDa band was not susceptible. Both denatured and native preparations were similarly susceptible to Endoglycosidase H (Figure 2A).

PNGase F cleaves glycans between the innermost N-acetylglucosamine and the protein, removing high mannose-, hybrid- and complex-type glycans. Treatment of cell lysates with PNGase F removed both the 90 kDa and 110 kDa FGFR4 bands, providing further evidence that they represent high mannose- or hybrid- and complex-type glycoforms, respectively (Figure 2B). Collectively, these data confirm that FGFR4 is N-glycosylated, identify the 90 kDa band as the high mannose- or hybrid-type glycan form, and identify the 110 kDa band as the complex-type form. We speculate that the doublet seen after deglycosylase treatment represents a non-glycan posttranslational modification to FGFR4. To determine whether the FGFR4 or R4-ICD bands observed following enzymatic deglycosylation represented different phosphorylation states of FGFR4, lysates were treated with lambda phosphatase. No obvious shifts of 80–110 kDa forms was seen. R4-ICD was largely converted to the faster of 2–3 forms at 45–50 kDa upon phosphatase treatment. Shifting seen for R4-ICD indicates the multiple bands of R4-ICD may represent different phosphorylation states of the protein (Figure 2C).

Next, live cells in culture were incubated with PNGase F in the media to enzymatically deglycosylate FGFR4 at the cell surface. Western blot analysis demonstrated that complex-type form of FGFR4 (110 kDa) shifted to an 85 kDa band, similar to deglycosylated FGFR4, while the high mannose- or hybrid-type (90 kDa) form persisted (Figure 2D). PNGase F enzyme is presumably excluded from the cell interior, thus deglycosylation is restricted to cell surface FGFR4, explaining the difference in the migration compared to Figure 2B. PNGase digestion for 1–2 hours resulted in increased R4-ICD signal, especially at ~50 kDa (Figure 2D). PNGase F treatment of live cells led to an approximately 3-fold increase in R4-ICD levels (Figure 2E). These data suggested that FGFR4 processing to R4-ICD was enhanced when N-linked glycans were removed.

HuCCT1-FGFR4 cells treated with NGI-1 (an inhibitor of oligosaccharyltransferase) showed a concentration-dependent loss of complex- and high mannose- or hybrid-type glycans (Figure 3A). Functionally, we observed reduced cytoprotective effect against TRAIL-induced apoptosis when N-glycosylation was completely inhibited (Figure 3B). When cells were treated with 10 μM NGI-1, we observed a partial decrease in glycosylation of the full length FGFR4 and increased R4-ICD levels (Figure 3A, both apparent R4-ICD bands), reminiscent of the increase we saw with PNGase F treatment (Figure 2D). These data suggest that deglycosylation (or partial deglycosylation) of FGFR4 promoted processing to R4-ICD. With a higher NGI-1 concentration (100 μM), FGFR4 was fully deglycosylated, and R4-ICD levels were not different than vehicle-treated cells. We treated cells with kifunensine, an inhibitor of mannosidase I, for 0–16 hours and observed a progressive loss of complex-type glycosylation of FGFR4 at 8 and 16 hours (Figure

3C). Interestingly, with partial deglycosylation (8 hours), we saw an increase in R4-ICD. Upon full effect (16 hours), there was no detectable complex-type FGFR4 and R4-ICD was no longer increased. These data are consistent with our interpretation that partial deglycosylation of N-glycosylated proteins may promote increased processing to R4-ICD. When cells were treated with PNGase F, the slowest migrating band of R4-ICD increased in intensity in KMCH cells, and both detectable bands increased in HuCCT1-FGFR4 cells (Figure 2D). NGI-1 treatment led to an increase in both detectable bands of R4-ICD and band resolution with kifunensine could not resolve if the increase was due to a single band or multiple R4-ICD forms. The multiple R4-ICD bands observed in Figures 1–4 may reflect distinct processing events in generating R4-ICD.

To promote FGFR4 processing to R4-ICD in the absence of protein synthesis and glycosylation changes, crude lysate was obtained (termed active lysate) and either frozen immediately or incubated at 37°C to allow endogenous proteases to act. Processing of FGFR4 to R4-ICD occurred with incubation (Figure 4A). Initial experiments using HuCCT1-FGFR4 cells were performed to determine if 20- or 60-minute incubation was required, and both were adequate. We tested processing to R4-ICD in active lysates of cells expressing mutant forms of FGFR4 to understand the role of each of the five glycosylation sites on proteolysis. This approach, in part, would allow us to determine if increased processing upon deglycosylation was due to glycosylation of FGFR4 or of another protein. Cell lines expressing the following forms of mutant FGFR4 were used: N112Q, N258Q, N290Q, N311Q, N322Q, and quadruple mutant 4Q (only 322 remained an asparagine). Two or three clones per FGFR4 mutant were used to account for clonal variation. Results were quantified as the ratio of R4-ICD to total FGFR4 and graphed (Figure 4B).

Blots used for quantification are shown in Figure 4C–H. Wild-type FGFR4 showed the highest amount of processing and preventing glycosylation at Asn-290 prevented increased R4-ICD levels. Mutant 4Q also showed no additional processing. FGFR4 mutants that could not be glycosylated at Asn-112, −258, −311, and −322 showed only a subtle decrease in processing to R4-ICD (Figure 4C, 4D, 4F, and 4G). Several FGFR4 mutants showed altered SDS-PAGE migration at 80–110kD compared to the wild-type FGFR4. In particular, the highest molecular weight form of FGFR4 in N258Q, N290Q, and 4Q mutants migrated faster than the highest molecular weight form of wild-type FGFR4 (Figure 4D, 4E, & 4H), suggesting that residues Asn-258 and Asn-290 contribute more to the mobility shift due to glycosylation. That may indicate that Asn-258 and Asn-290 are main glycosylation sites or that they prime additional sites for N-linked glycosylation. The 110 kDa band did not show a strong migration shift in N112Q, N311Q, or N322Q mutants (Figure 4C, 4F, & 4G), suggesting these sites are not dominant glycosylation sites in this cholangiocarcinoma cell line. The 4Q mutant (which contains mutations at both Asn-258 and −290—as well as Asn-112 and −311) migrated fastest on the gel, consistent with a cumulative effect of preventing glycosylation at multiple sites (Figure 4H). None of the Asn-to-Gln mutants caused increased processing. Thus, while deglycosylation in the whole cell increased R4-ICD formation, we could not replicate this effect with FGFR4 glycomutants.

We considered that glycomutants may not be trafficked properly. Figure 5A shows a representative anti-FGFR4 immunofluorescence image of several cell lines: cells expressing

FGFR4 through stable transfection with cDNA (top two panels; HuCCT-FGFR4) or two separate cell lines with endogenous expression of FGFR4 (bottom two panels; KMCH and Mz-ChA-1). We observed cytoplasmic staining for FGFR4 for endogenous or transfected FGFR4 with punctate or vesicle-like staining intracellularly. FGFR4 was not predominantly localized to the plasma membrane. The top two images in Figure 5A represent two different optical planes in the z axis for a single cell (0.6 μM difference between two images). With optical sectioning, we noted that plasma membrane FGFR4 was observed near the coverslip (white arrows in Figure 5A) and in most optical planes FGFR4 was distributed in the cell with apparent structural complexity. Images collected from HuCCT1 parental cells parental or HuCCT1 cells expressing wild-type or mutant FGFR4 are shown in Figure 5B. Parental cells lack FGFR4 and, as expected, did not show signal in immunofluorescence. In cells expressing wild-type FGFR4, staining appeared not only at the plasma membrane but especially was distributed intracellularly. Cells expressing N258Q, N290Q, N311Q, or N322Q resembled the wild-type FGFR4 distribution while N112Q showed a region of concentrated staining adjacent to the nucleus (Figure 5B). We performed dual immunofluorescence on wild-type, N112Q, and 4Q cell lines for FGFR4 and a Golgi marker, giantin. N112Q FGFR4 partially colocalized with giantin at the Golgi (yellow; Figure 5C).

We next tested if any of the FGFR4 glycomutants showed altered cell migration or resistance to cell death. All of the clones supported migration similar to wild-type FGFR4. A single clone of the N112Q mutant (5A3) showed significantly reduced migration compared to a single clone each of N258Q (3B3) and N311Q (8A3), but none of the clones were different than wild-type and no additional statistical differences were observed. Thus, each mutant was capable to promote a similar migratory effect as wild-type (Figure 6A). Representative images of migrated HuCCT-FGFR4 cells, and one clone each of N112Q and N258Q mutants (selected because they showed the range of lowest and highest migration) are shown in Figure 6B–D.

Next, caspase activity was measured after challenge with chemotherapeutics or staurosporine. Parental HuCCT1 cells lacking endogenous FGFR4 were sensitive to apoptosis (Figure 6E, F). Wild-type FGFR4 efficiently protected cancer cells from chemotherapy-induced apoptosis. Cell lines expressing mutant FGFR4 were mostly protected from chemotherapy-induced cell death compared to HuCCT1 parental cells, but to a lesser extent than wild-type FGFR4. The N322Q mutation had the least protection (Figure 6E), and the 4Q mutant was also relatively poor at cytoprotection (Figure 6F). Mutant cell lines expressing FGFR4 N322 or 4Q did not provide any statistical survival benefit to cells compared to parental HuCCT1 cells in staurosporine-treated cells. Overall, most of the glycomutants offered at least partial cytoprotection. Data regarding the effects of Asn-to-Gln mutations on FGFR4 cleavage, cell migration, and apoptosis resistance are summarized in Table 2.

Discussion

FGFR signaling has received increased attention in cholangiocarcinoma. Data in this manuscript primarily relate to how glycosylation regulates the processing, function, and

localization of FGFR4. We demonstrated that non-specific deglycosylation or blocking of glycosylation increased processing of FGFR4 to a proteolytic fragment, R4-ICD. Individual and combined glycomutants of FGFR4 did not recapitulate this increased processing, suggesting the effect is not due to deglycosylation of FGFR4 itself. All mutants supported cell migration while selected mutants were less efficient at protecting from apoptosis. Overall, these data show that glycosylation helps to regulate the processing, signaling, and localization of FGFR4 in cholangiocarcinoma cells. Each of these roles will be discussed here.

Processing of FGFR4 to R4-ICD is only recently recognized (Merilahti, et al., 2017; Huang, et al., 2009), and the product corresponds to the kinase domain, separated from the regulation of the ligand-binding region. We showed R4-ICD production from endogenous (KMCH) and transgenic FGFR4 and that R4-ICD is the predominant form of FGFR4 in human cholangiocarcinoma tumor samples. The rationale for studying the role of glycosylation in FGFR4 processing is two-fold. First, activation of FGFR3 was necessary for its cleavage (Degnin, et al., 2011). Second, Notch signaling (a proteolysis-driven event) is regulated by receptor glycosylation (Bruckner, et al., 2000). Complex-type glycosylated FGFR4 was the functional form for regulating cholesterol biosynthesis (Triantis, et al., 2010). We reasoned that FGFR4 glycosylation may influence receptor activation and R4-ICD production. Indeed, we observed increased R4-ICD with deglycosylation.

Removal of N-linked sugars by enzyme treatment or blocking glycosylation by small molecule inhibitors of N-linked glycosylation promoted processing of FGFR4 to R4-ICD. This prompted consideration that post-translational glycosylation of FGFR4 itself could regulate processing to R4-ICD. Alternatively, non-selective removal or inhibition of glycosylation may affect another target and indirectly regulate R4-ICD production. Importantly, the enzymatic removal of glycans in living cells will naturally occur along with new synthesis (and potentially new processing) of FGFR4. Thus, we cannot distinguish whether R4-ICD comes from newly synthesized/glycosylated FGFR4 or from FGFR4 that has been deglycosylated at the membrane. To help resolve both the direct versus indirect effect, and the role of newly synthesized versus recently deglycosylated FGFR4 in producing R4-ICD, we produced FGFR4 mutants that lacked the ability to be glycosylated at selected sites.

Each predicted Asn site of glycosylation was tested for processing to R4-ICD. R4-ICD was observed in all mutants, at some level. However, additional processing in the incubated samples was not strong (N290) or was absent (4Q) in two mutants. This data may indicate that processing is slower in the N290Q and 4Q mutant cells (and somewhat slower in N112Q, N258Q, N311Q, and N322Q). It still occurs, as R4-ICD is seen in cell lysate, but loss of glycosylation may reduce the sensitivity to protein cleavage. Importantly, we did not find that a specific glycosylation site was responsible for increasing processing, despite seeing more R4-ICD after deglycosylation of the cell. Still, with five potential glycosylation sites, there are 32 potential glycosylation mutant combinations; our experiments included seven of these. It remains plausible that a particular pattern of glycomutants could demonstrate increased processing.

It should also be noted that several FGFR4 mutants ran at noticeably different molecular weights than the WT FGFR4. In particular, FGFR4 N258Q, N290Q and 4Q full length FGFR4 appeared to run more quickly than WT FGFR4, suggesting that residues 258 and 290 are more highly glycosylated. The 4Q mutant (which contains mutations at residues 258 and 290, in addition to 112 and 311) appeared to run the quickest on the gel, suggesting a cumulative effect of preventing glycosylation at multiple sites.

Regarding signaling, FGFR4 promoted cancer cell survival. One limitation of our study is that using NGI-1 to inhibit glycosylation is not specific to FGFR4. Thus, we cannot establish that the apoptosis sensitization seen when we treated cells with 100 μM NGI-1 was due to loss of glycosylated FGFR4, versus an effect of NGI-1 on a different target. However, we do observe increased sensitization to cell death in N322Q and 4Q mutants, further supporting the role of glycosylation on FGFR4's cytoprotective effects.

In general, glycosylation mutants of FGFR4 were less cytoprotective than wild-type FGFR4. However, cells expressing mutant FGFR4 were still more protected than cells lacking FGFR4. The two mutants that provided the least protection were FGFR4 N322Q and 4Q. These two mutants have opposing effects on glycosylation—N322Q can be glycosylated at all sites except Asn-322, while 4Q can only be glycosylated at position 322. The observation that these two mutants had the least protection from cell death suggests that position 322 dominated the survival signaling, and to match the defect requires that all other glycosylation sites be changed. Glycosylation at position N322 may be a strong determinant of survival function. One possible explanation for this high dependence upon glycosylation at position 322 relates to its proximity to FGFR4's transmembrane domain, amino acids 370–390, affecting conformational signaling to the intracellular domain. Alternatively, it's possible that glycosylation at Asn-322 facilitates ligand binding.

Glycosylation of FGFR4 largely did not affect protein localization. Cells expressing N112Q and 4Q mutants of FGFR4 had the most unique staining and N112Q had a portion that colocalized at or near the Golgi. Notably, the staining of cells showed FGFR4 that was not confined to the plasma membrane. Localization of FGFR4 in immunofluorescence experiments revealed staining that was localized to the intracellular compartment, consistent with intracellular vesicles. When cells were imaged closer to the coverslip, we observed the expected localization to the plasma membrane. We visualized FGFR4 in cells with endogenous expression and found a similar pattern of intracellular puncta, consistent with intracellular vesicles. Reports of FGFR4 localization and internalization showed a similar distribution by immunofluorescent staining (Haugsten, et al., 2005), and interaction of FGFR4 with intracellular trafficking and endosomal proteins (Haugsten, et al., 2016). We have not observed any non-specific staining in cells lacking FGFR4, so this distribution may reflect immunofluorescence detection of the membrane-bound full-length receptor as well as the processed R4-ICD.

Despite initial data that glycosylation of FGFR4 might enhance processing to R4-ICD, our glycomutants did not support such direct regulation. Future studies on proteolytic regulation and regulation of apoptotic signaling may help define R4-ICD production and significance in cholangiocarcinoma.

Supplementary Material

Refer to Web version on PubMed Central for supplementary material.

Acknowledgements:

Supported by the National Cancer Institute (NCI) of the National Institutes of Health, award number R01CA222649 (JLM). Additional support from the Fred & Pamela Buffett Cancer Center. AJP was supported by a UNMC Graduate Student Fellowship. We thank the University of Nebraska Medical Center Advanced Microscopy Core Facility. The Advanced Microscopy Core facility receives partial support from the National Institute for General Medical Science (NIGMS) INBRE - P20GM103427 and COBRE - P30GM106397 grants, as well as support from the NCI for The Fred & Pamela Buffett Cancer Center Support Grant- P30CA036727, and the Nebraska Research Initiative. This publication's contents and interpretations are the sole responsibility of the authors and do not necessarily represent the official views of the NIH.

Abbreviations:

Asn	Asparagine
FGF	Fibroblast growth factor
FGFR	Fibroblast growth factor receptor
NGI-1	N-linked glycosylation inhibitor 1
PNGase	F: Peptide:N-glycosidase F
R4-ICD	FGFR4 intracellular domain
Ser	Serine
Thr	Threonine

References:

Arauz E, Aggarwal V, Jain A, Ha T, & Chen J (2016). Single-Molecule Analysis of Lipid–Protein Interactions in Crude Cell Lysates. Analytical Chemistry, 88(8), 4269–4276. [PubMed: 27015152]

Brückner K, Perez L, Clausen H, & Cohen S (2000). Glycosyltransferase activity of Fringe modulates Notch–Delta interactions. Nature, 406(6794), 411–415. [PubMed: 10935637]

Citores L, Bai L, Sørensen V, & Olsnes S (2007). Fibroblast growth factor receptor-induced phosphorylation of STAT1 at the golgi apparatus without translocation to the nucleus. Journal of Cellular Physiology, 212(1), 148–156. [PubMed: 17311277]

Degnin CR, Laederich MB, & Horton WA (2011). Ligand activation leads to regulated intramembrane proteolysis of fibroblast growth factor receptor 3. Molecular Biology of the Cell, 22(20), 3861–3873. [PubMed: 21865593]

Haugsten EM, Sørensen V, Brech A, Olsnes S, & Wesche J (2005). Different intracellular trafficking of FGF1 endocytosed by the four homologous FGF receptors. Journal of cell science, 118(17), 3869–3881. [PubMed: 16091423]

Haugsten EM, Sørensen V, Kunova Bosakova M, De Souza GA, Krejci P, Wiedlocha A, & Wesche J (2016). Proximity labeling reveals molecular determinants of FGFR4 endosomal transport. Journal of proteome research, 15(10), 3841–3855. [PubMed: 27615514]

Huang X, Yang C, Jin C, Luo Y, Wang F, & McKeehan WL (2009). Resident hepatocyte fibroblast growth factor receptor 4 limits hepatocarcinogenesis. Molecular Carcinogenesis: Published in cooperation with the University of Texas MD Anderson Cancer Center, 48(6), 553–562.

Justus CR, Leffler N, Ruiz-Echevarria M, & Yang LV (2014). In vitro cell migration and invasion assays. Journal of Visualized Experiments: JoVE, (88).

Lee JY, Park YN, Uhm KO, Park SY, & Park SH (2004). Genetic alterations in intrahepatic cholangiocarcinoma as revealed by degenerate oligonucleotide primed PCR-comparative genomic hybridization. Journal of Korean Medical Science, 19(5), 682–687. [PubMed: 15483344]

Lin BC, Wang M, Blackmore C, & Desnoyers LR (2007). Liver-specific activities of FGF19 require Klotho beta. Journal of Biological Chemistry, 282(37), 27277–27284.

Massironi S, Pilla L, Elvevi A, Longarini R, Rossi RE, Bidoli P, & Invernizzi P (2020). New and emerging systemic therapeutic options for advanced cholangiocarcinoma. Cells, 9(3), 688.

Meijer D, Sieuwerts AM, Look MP, van Agthoven T, Foekens JA, & Dorssers LC (2008). Fibroblast growth factor receptor 4 predicts failure on tamoxifen therapy in patients with recurrent breast cancer. Endocrine-Related Cancer, 15(1), 101. [PubMed: 18310279]

Merilahti JA, Ojala VK, Knittle AM, Pulliainen AT, & Elenius K (2017). Genome-wide screen of gamma-secretase–mediated intramembrane cleavage of receptor tyrosine kinases. Molecular Biology of the Cell, 28(22), 3123–3131. [PubMed: 28904208]

Nakamura H, Arai Y, Totoki Y, Shirota T, Elzawahry A, Kato M, Hama N, Hosoda F, Urushidate T, Ohashi S, Hiraoka N, Ojima H, Shimada K, Okusaka T, Kosuge T, Miyagawa S, and Shibata T (2015). Genomic spectra of biliary tract cancer. Nature Genetics, 47(9), 1003–1010. [PubMed: 26258846]

Ornitz DM, & Itoh N (2015). The fibroblast growth factor signaling pathway. Wiley Interdisciplinary Reviews: Developmental Biology, 4(3), 215–266. [PubMed: 25772309]

Razumilava N, & Gores GJ (2014). Cholangiocarcinoma. The Lancet, 383(9935), 2168–2179.

Rizvi S, Khan SA, Hallemeier CL, Kelley RK, & Gores GJ (2018). Cholangiocarcinoma—evolving concepts and therapeutic strategies. Nature Reviews Clinical Oncology, 15(2), 95–111.

Rodgers KJ, & Dean RT (2003). Assessment of proteasome activity in cell lysates and tissue homogenates using peptide substrates. The International Journal of Biochemistry & Cell Biology, 35(5), 716–727. [PubMed: 12672463]

Sia D, Hoshida Y, Villanueva A, Roayaie S, Ferrer J, Tabak B, Peix J, Sole M, Tovar V, Alsinet C and Cornella H, Klotzle B, Fan J-B, Cotsoglou C, Thung SN, Fuster J, Waxman S, Garcia–Valdecasas JC, Bruix J, Schwartz ME, Beroukhim R, Mazzaferro V, & Llovet JM (2013). Integrative molecular analysis of intrahepatic cholangiocarcinoma reveals 2 classes that have different outcomes. Gastroenterology, 144(4), 829–840. [PubMed: 23295441]

Takeuchi H, & Haltiwanger RS (2014). Significance of glycosylation in Notch signaling. Biochemical and Biophysical Research Communications, 453(2), 235–242. [PubMed: 24909690]

Taylor JG VI, Cheuk AT, Tsang PS, Chung JY, Song YK, Desai K, … & Khan J (2009). Identification of FGFR4-activating mutations in human rhabdomyosarcomas that promote metastasis in xenotransplanted models. The Journal of Clinical Investigation, 119(11), 3395–3407. [PubMed: 19809159]

Taylor P, Takeuchi H, Sheppard D, Chillakuri C, Lea SM, Haltiwanger RS, & Handford PA (2014). Fringe-mediated extension of O-linked fucose in the ligand-binding region of Notch1 increases binding to mammalian Notch ligands. Proceedings of the National Academy of Sciences, 111(20), 7290–7295.

Tiong KH, Tan BS, Choo HL, Chung FFL, Hii LW, Tan SH, … & Leong CO (2016). Fibroblast growth factor receptor 4 (FGFR4) and fibroblast growth factor 19 (FGF19) autocrine enhance breast cancer cells survival. Oncotarget, 7(36), 57633. [PubMed: 27192118]

Triantis V, Saeland E, Bijl N, Oude-Elferink RP, & Jansen PL (2010). Glycosylation of fibroblast growth factor receptor 4 is a key regulator of fibroblast growth factor 19–mediated down-regulation of cytochrome P450 7A1. Hepatology, 52(2), 656–666. [PubMed: 20683963]

Tuominen H, Heikinheimo P, Loo BM, Kataja K, Oker-Blom C, Uutela M, … & Goldman A (2001). Expression and glycosylation studies of human FGF receptor 4. Protein Expression and Purification, 21(2), 275–285. [PubMed: 11237689]

Valle J, Wasan H, Palmer DH, Cunningham D, Anthoney A, Maraveyas A, … & Bridgewater J (2010). Cisplatin plus gemcitabine versus gemcitabine for biliary tract cancer. New England Journal of Medicine, 362(14), 1273–1281.

Vasilieva LE, Papadhimitriou SI, Alexopoulou A, Pavlidis D, Kostopoulos I, Georgiakaki M, … & Dourakis SP (2013). An extended fluorescence in situ hybridization approach for the cytogenetic study of cholangiocarcinoma on endoscopic retrograde cholangiopancreatography brushing cytology preparations. Human pathology, 44(10), 2173–2179. [PubMed: 23845469]

Wu X, Ge H, Gupte J, Weiszmann J, Shimamoto G, Stevens J, … & Li Y (2007). Co-receptor requirements for fibroblast growth factor-19 signaling. Journal of Biological Chemistry, 282(40), 29069–29072.

Xu YF, Yang XQ, Lu XF, Guo S, Liu Y, Iqbal M, … & Chen YX (2014). Fibroblast growth factor receptor 4 promotes progression and correlates to poor prognosis in cholangiocarcinoma. Biochemical and biophysical research communications, 446(1), 54–60. [PubMed: 24565842]

Yi F, Amarasinghe B, & Dang TP (2013). Manic fringe inhibits tumor growth by suppressing Notch3 degradation in lung cancer. American journal of cancer research, 3(5), 490. [PubMed: 24224126]

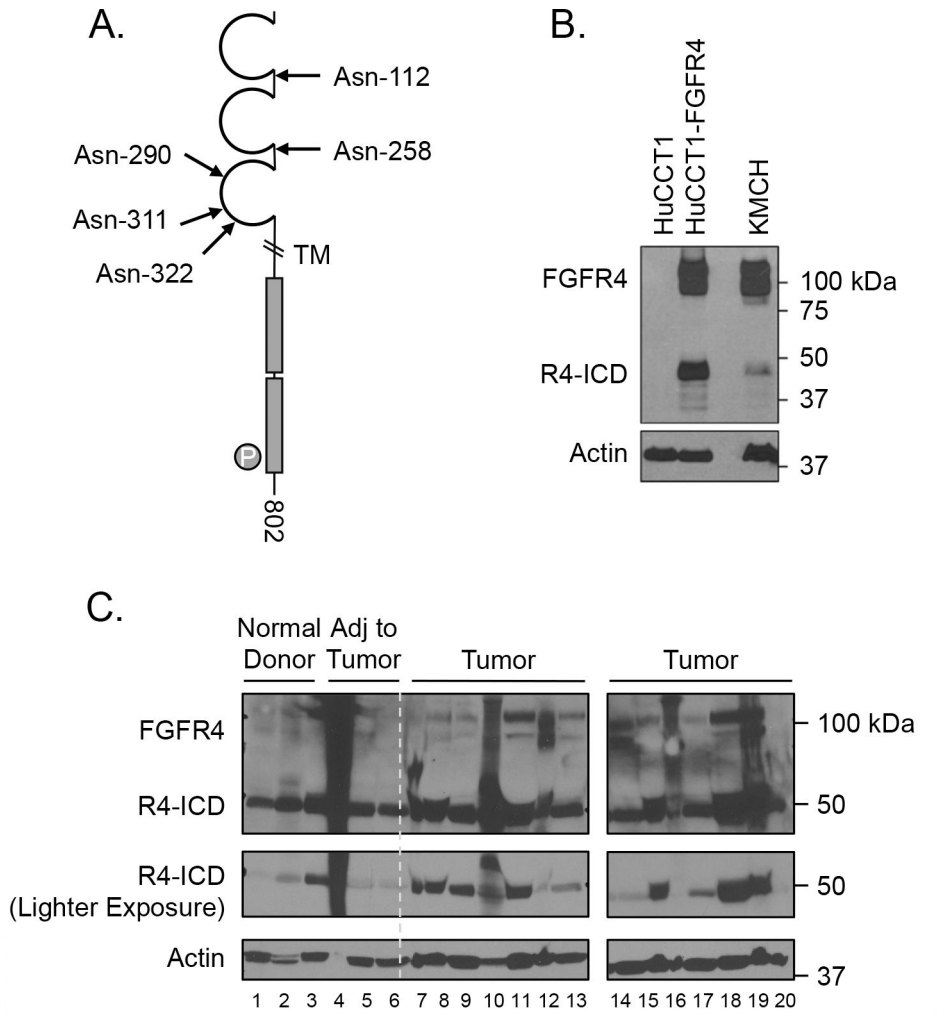

Figure 1. FGFR4 glycosylation in cholangiocarcinoma.

A. Schematic of FGFR4 showing five predicted N-linked glycosylation sites, the transmembrane (TM) domain and the intracellular C-terminal kinase domain. B. HuCCT1, HuCCT1-FGFR4, and KMCH cells were blotted for FGFR4. Full-length receptor is visualized at 90–110 kDa and R4-ICD is observed as signal around 45–50 kDa; representative of n=3. C. FGFR4/R4-ICD protein expression in three healthy (donor) liver samples, three non-tumor samples adjacent to liver cancer (Adj to tumor), and fourteen human cholangiocarcinoma tumor samples. Lane numbers correspond to numbers in table 1.

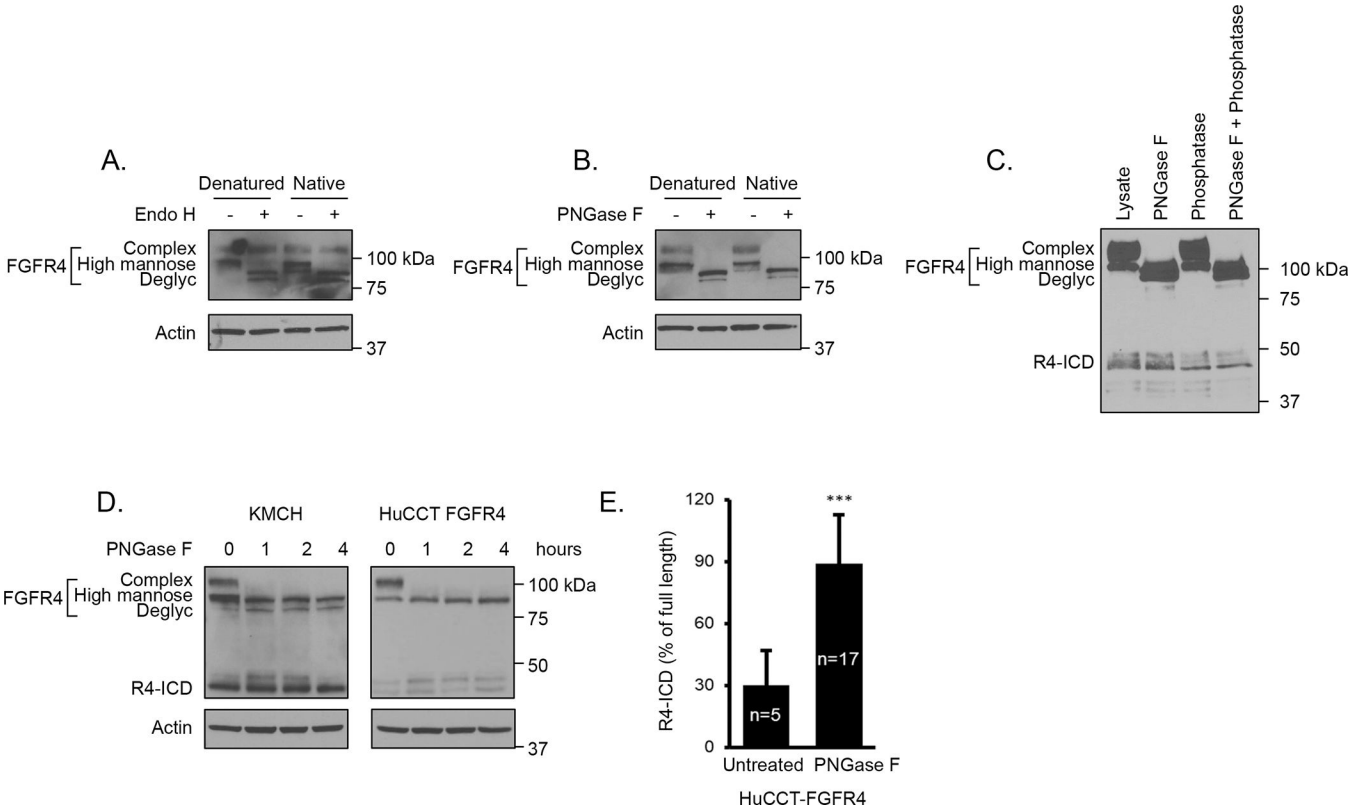

Figure 2. FGFR4 deglycosylation increased R4-ICD production.

A. Endoglycosidase H treatment of HuCCT1-FGFR4 cell lysates. The band labeled "Deglyc" represents the deglycosylated form of FGFR4. B. PNGase F treatment of HuCCT1-FGFR4 cell lysate. C. Treatment of HuCCT1-FGFR4 cell lysates with both PNGase F and Lambda phosphatase. D. KMCH and HuCCT1-FGFR4 cells were treated with PNGase F in the culture media. E. R4-ICD-to-full-length FGFR4 (percent) was averaged from untreated and PNGase F-treated HuCCT1-FGFR4 cells total sample number quantified is indicated on graph. A-C; n=3, D; KMCH: n=3, HuCCT1-FGFR4: n=5, E; n=5. ***p <0.001.

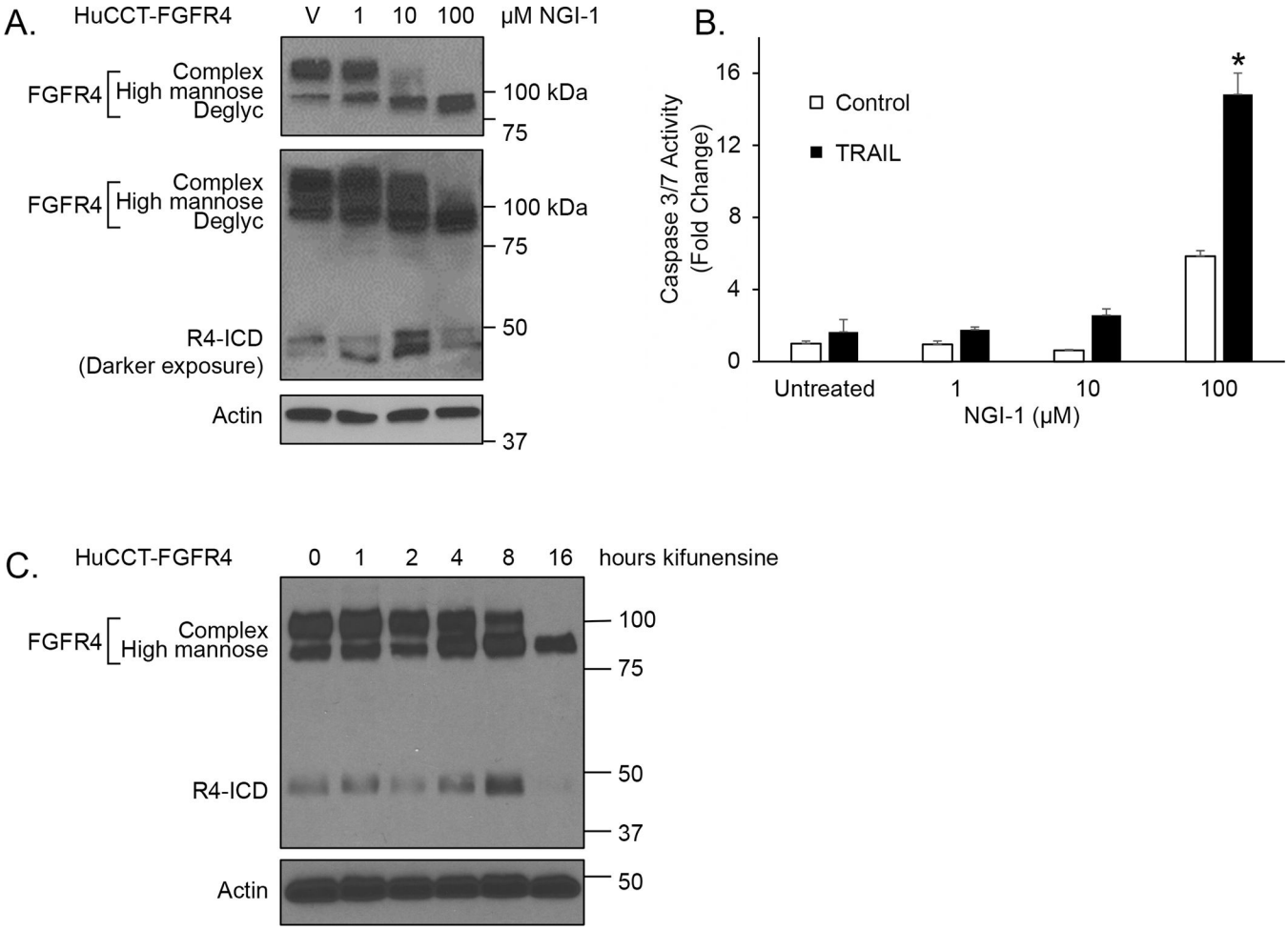

Figure 3. NGI-1 treatment reduced FGFR4 glycosylation and cytoprotection.

A. HuCCT1-FGFR4 cells were treated with vehicle (“V”) or NGI-1 overnight, at the indicated concentrations. n=3. B. Caspase activity was measured on HuCCT1-FGFR4 cells treated overnight with NGI-1 followed by a 6-hour treatment with 10 ng/mL TRAIL. Quadruplicate samples measured, repeated twice; representative data shown. * $p<0.05$. C. HuCCT FGFR4 cells were treated with kifunensine, 5 μM, for 0–16 hours. This was performed three times, and a representative blot is shown.

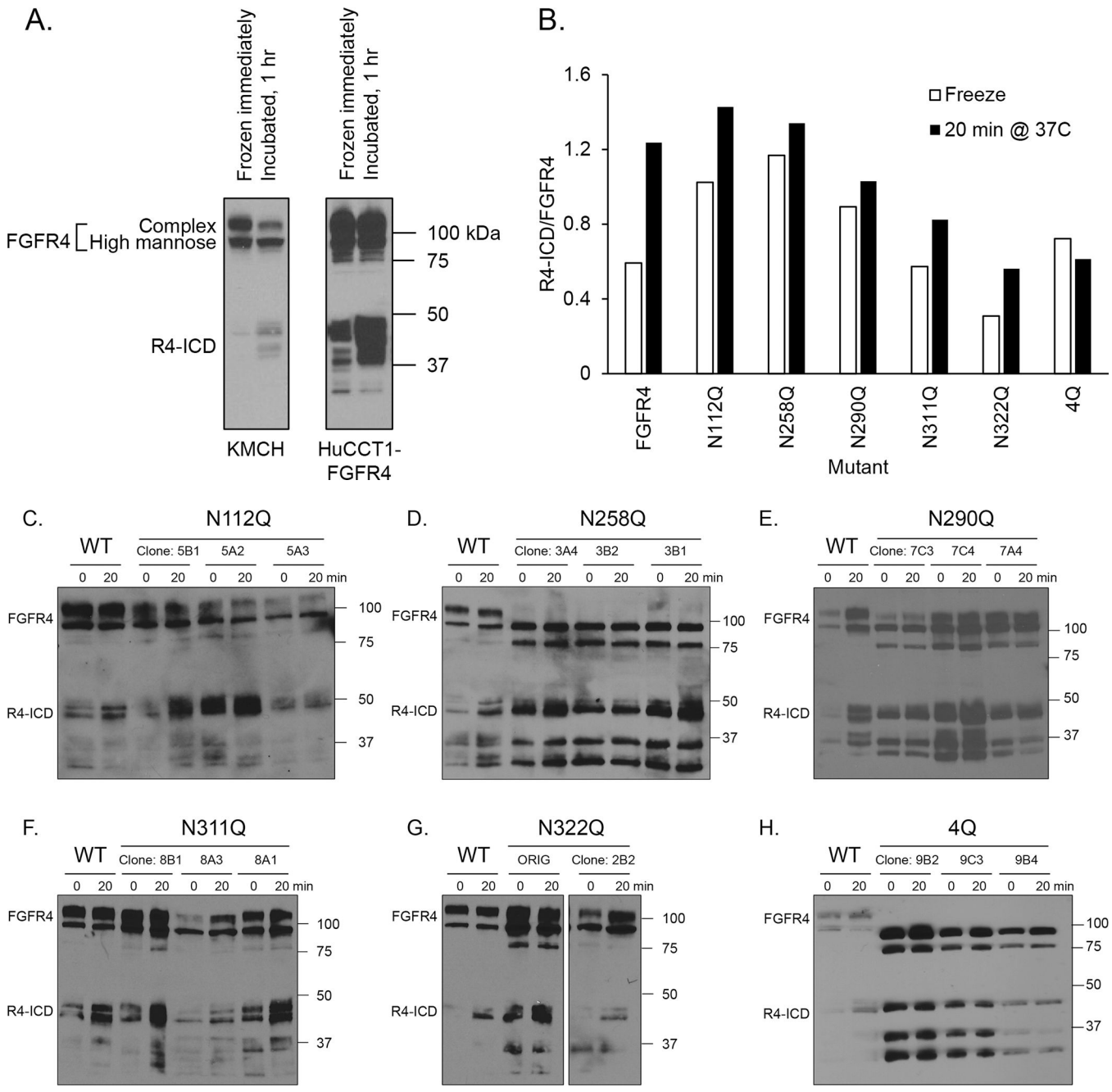

Figure 4. Mutation of selected glycosylation sites reduced processing of FGFR4 to R4-ICD.

A. Active cell lysates for KMCH and HuCCT1-FGFR4 cells were either frozen immediately or incubated at 37°C for 1 hour. n=5. B. Active lysates of cells expressing glycosylation mutants of FGFR4 were incubated to measure processing to R4-ICD. Three selected clones for each mutant (except N322Q where we had two clones) were averaged. R4-ICD/FGFR4 ratio is graphed. C-H: Western blot analysis of active cell lysates collected from clonal cell lines expressing mutant forms of FGFR4 are shown. Labels directly over the blot indicate if the sample was frozen immediately after collecting (0) or incubated for 20 minutes at 37°C prior to freezing (20). Additionally, the location of the FGFR4 mutation and individual clone

numbers are indicated. Each blot has wild-type (WT) FGFR4 in lanes one and two to serve as a molecular weight and processing comparison.

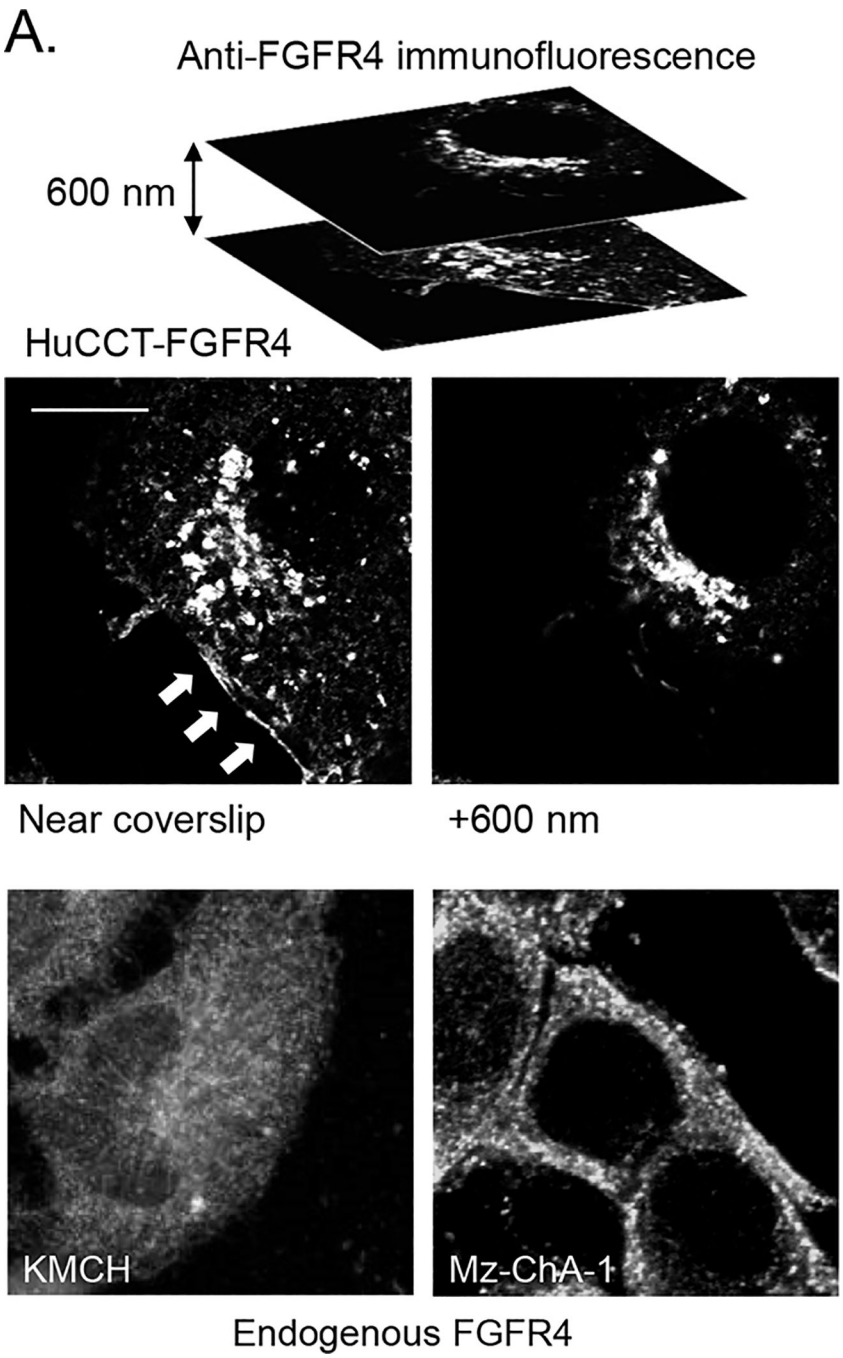

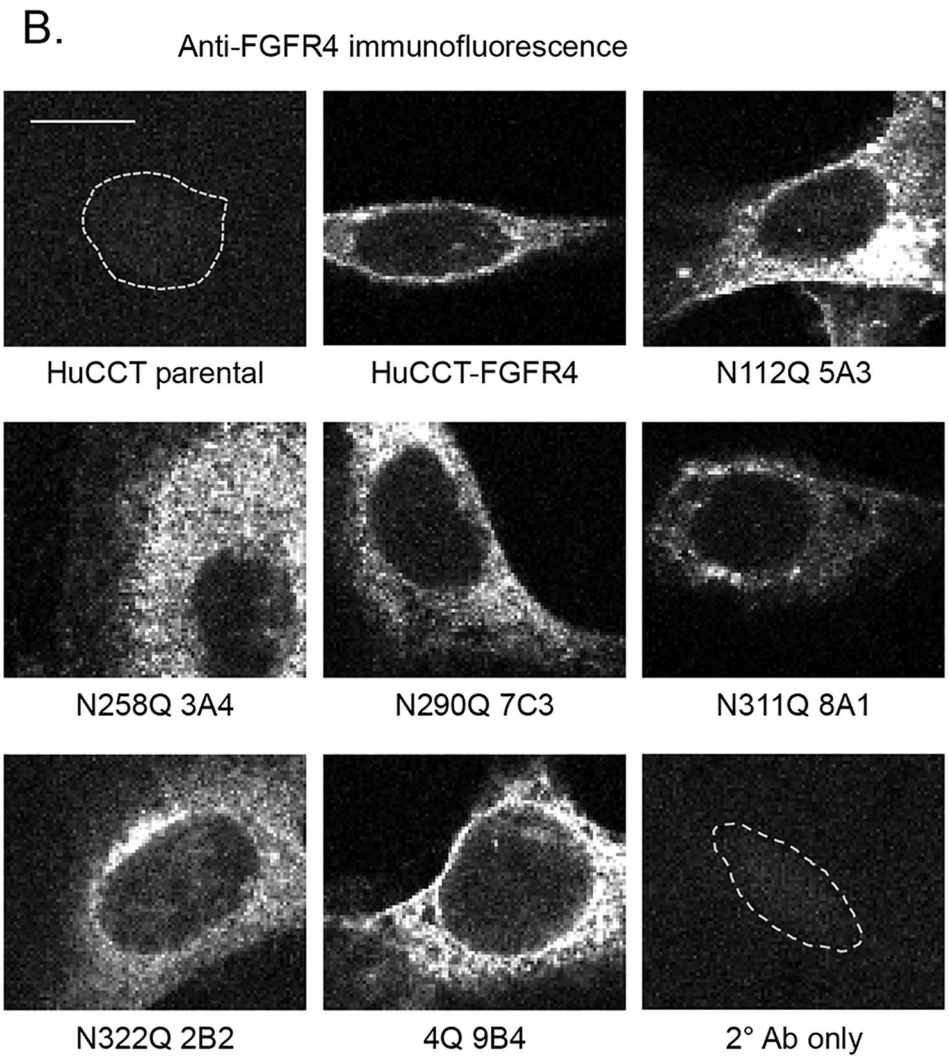

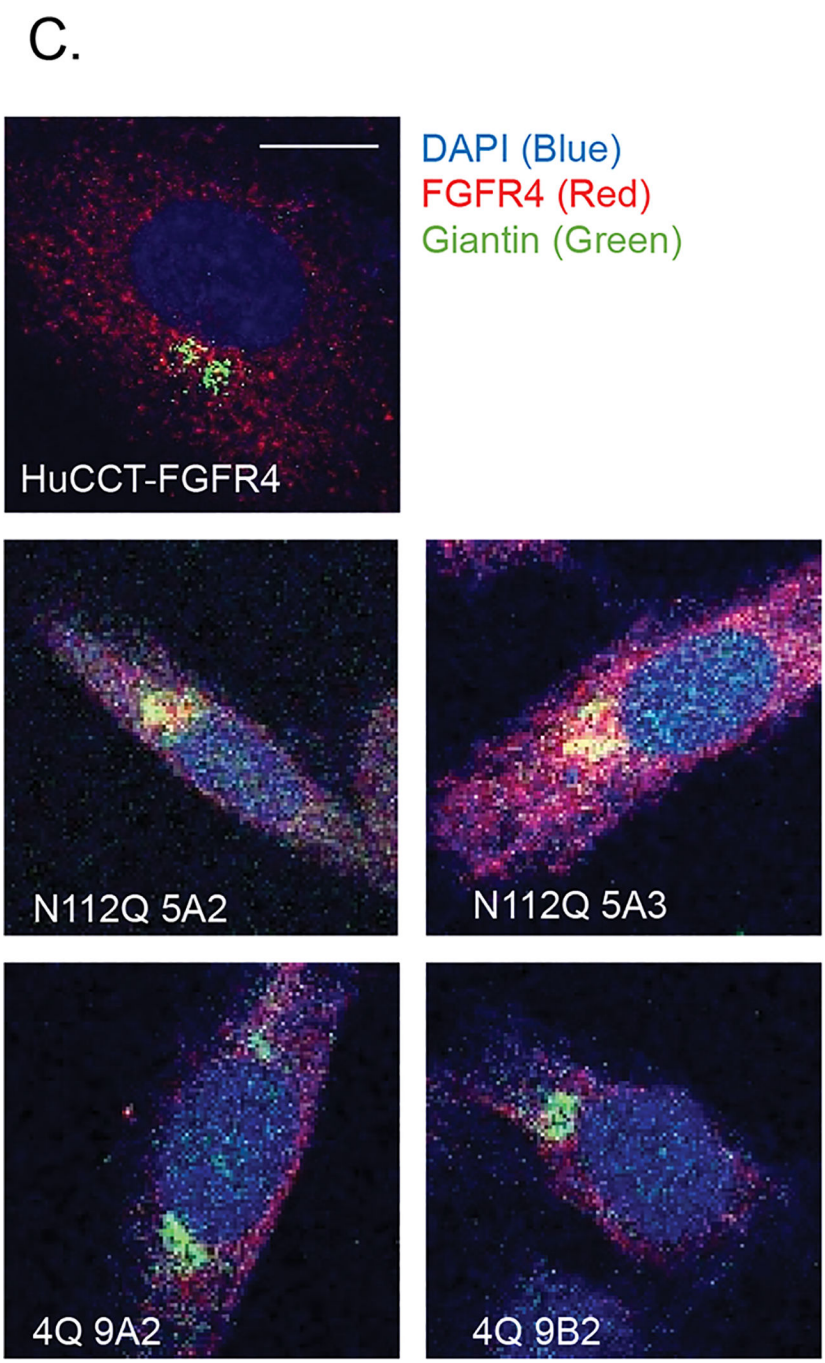

Figure 5. Cellular localization of wild-type and mutant FGFR4.

A. Immunofluorescence for FGFR4 (white) in cells with exogenous (HuCCT-FGFR4; top panels) or endogenous (KMCH, Mz-ChA-1; bottom panels) FGFR4 was performed. The HuCCT1-FGFR4 panels are images of the same cell with a difference in the z-plane of 0.6 μM to demonstrate membrane staining for FGFR4 (arrows, left panel). B. FGFR4 immunofluorescence of cells expressing wild-type or mutant FGFR4, site of mutation and clone number indicated below each panel. FGFR4 shown in white. Parental HuCCT cells do not have FGFR4 signal and secondary-only control showed no non-specific fluorescence.

C. Immunofluorescence for both FGFR4 (red) and giantin (green) was performed on cells expressing wild-type FGFR4 and mutants N112Q and 4Q. A-C: Representative images are shown, bar = 10 μm.

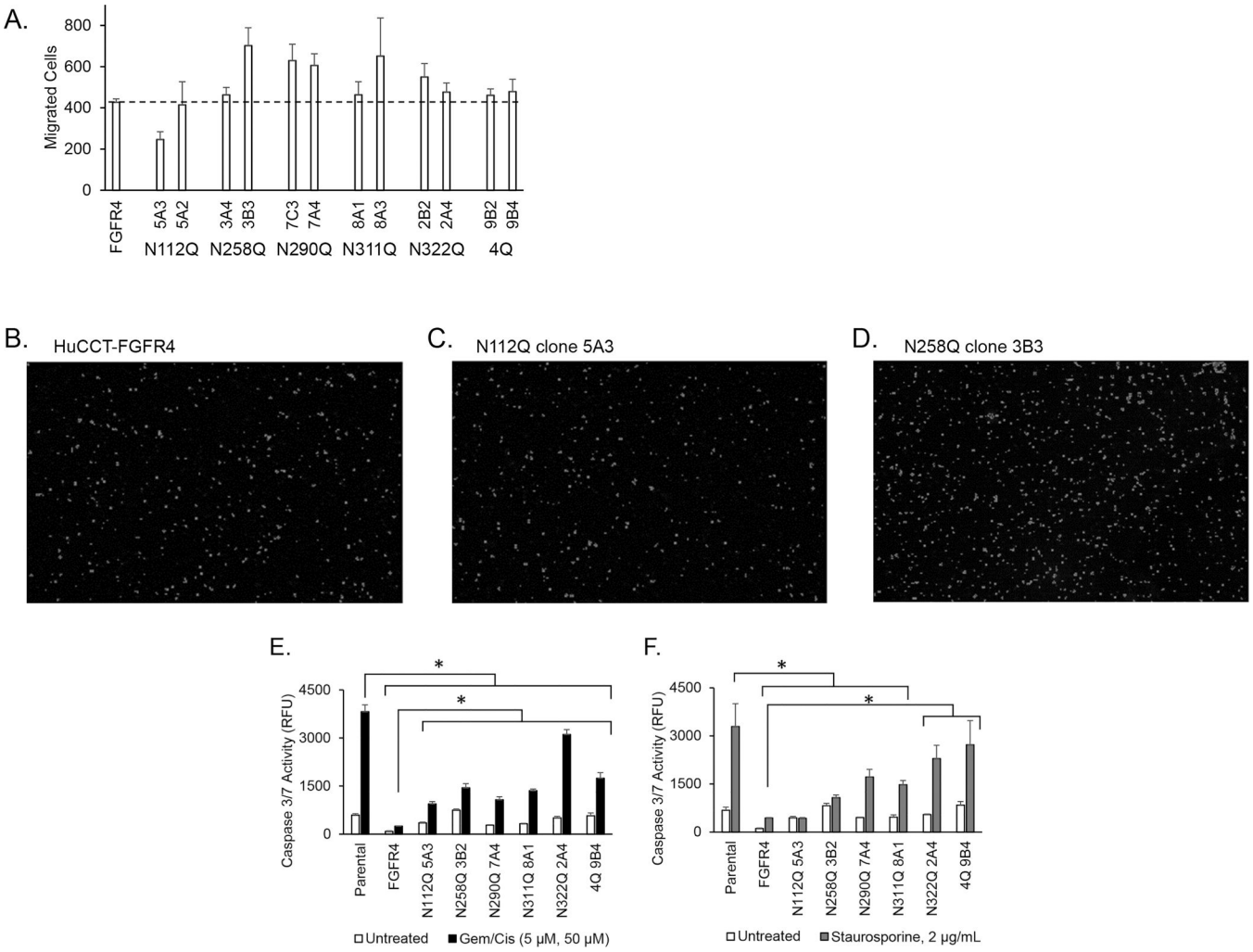

Figure 6. Migration and apoptosis of cells expressing FGFR4 glycomutants.

A. Two clones for each mutant were tested for migration over 24 h by transwell assay. n=3, mean ± SEM. No clones showed a statistically significant difference from wild-type (ANOVA with Bonferroni *post hoc*). B-D. Representative fields of migrated cells are shown from HuCCT-FGFR4 cells, N112Q 5A3 cells (least migration), and N258Q 3B3 cells (most migration). E, F. One clone for each mutant was treated with gemcitabine and cisplatin (5 μM and 50 μM, respectively, panel E), or staurosporine (2 μg/mL, panel F) for 24 hours. HuCCT1 cells lacking FGFR4 are labeled parental. n=4, mean ± SEM. Only treated (filled) samples were compared statistically to parental and to cells expressing wild-type FGFR4. * $p < 0.05$, ANOVA with Bonferroni *post hoc*.

Table 1.

Patient characteristics for 6 non-tumor livers and 14 tumor samples were utilized in this study.

Lane	Normal donor liver	Age	Sex	Anatomic site	Notes	Histologic grade (differentiated)	AJCC stage
1	ND1			liver	transplant (donor)		
2	ND2			liver	transplant (donor)		
3	ND3			liver	transplant (donor)		
	Adjacent normal tissue	**Age**	**Sex**	**Anatomic site**	**Notes**	**Histologic grade (differentiated)**	**AJCC stage**
4	N1			liver	adjacent to HCC		
5	N2#			liver	adjacent to cholangiocarcinoma		
6	N3*			liver	adjacent to cholangiocarcinoma		
	Tumor	**Age**	**Sex**	**Anatomic site**	**Notes**	**Histologic grade (differentiated)**	**AJCC stage**
7	T6#	72	F	liver	intrahepatic		pT2a, pN0, pMX
8	T5*	64	M	liver		moderately	pT3, pN0, pMX
9	T1	59	F	liver	intrahepatic	moderately to poorly	T2, N0, MX
10	T2	55	M	liver	intrahepatic	well	pT2, pN0, pMX
11	T3	52	F	liver		moderately	pT1, NX, MX
12	T4	50	F	liver	multiple tumors within the hepatic parenchyma	moderately	T3, N0, MX
13	T7	63	F	liver	intrahepatic		
14	T8	66	M	liver	intrahepatic	poorly	pT1, NX, MX
15	T9	50	M	gallbladder	gallbladder (met)	moderately	pT3, pN1
16	T10	32	M	liver		moderately	pT2a, pN0, pMX
17	T11	65	F	pancreas	pancreas (met)	moderately	pT3, pN1
18	T12	69	M	liver	intrahepatic	well	pT1a, NX, MX
19	T13	72	F	liver	intrahepatic	poorly	pT2, NX, MX
20	T14	72	F	liver	Intrahepatic	moderately	pT2, pN0, pMX

# Indicates that liver sample N2 and tumor T6 were from different regions of the same liver.

* Indicates that liver sample N3 and tumor T5 were from different regions of the same liver.

Table 2.

Summary of the glycomutants and their effects on R4-ICD production, cell migration, and resistance to apoptosis. The degree of each activity observed is indicated on a relative scale from zero to 3+.

	FGFR4	N112Q	N258Q	N290Q	N311Q	N322Q		4Q
Cleavage to R4-ICD	+++	++	+	0	++	++		0
Migration	++	+	++	+++	++	++		++
Cytoprotection Against Gemcitabine/Cisplatin	+++	++	++	++	++	+		++
Cytoprotection Against Staurosporine	+++	+++	++	++	++	+		+